Raman Scattering of 4-Aminobenzenethiol Sandwiched between Ag/Au Nanoparticle and Macroscopically Smooth Au Substrate

Kwan Kim* and Jae Keun Yoon

Laboratory of Intelligent Interfaces, School of Chemistry, Seoul National University, Seoul 151-742, Korea

Received: May 28, 2005; In Final Form: September 15, 2005

Raman scattering measurements were conducted for a 4-aminobenzenethiol (4-ABT) monolayer assembled on a macroscopically smooth Au substrate. Although no peak was detected at the beginning, Raman peaks were distinctly observed by attaching Ag or Au nanoparticles onto the 4-ABT monolayer (Ag(Au)@4-ABT/Au(flat)). Considering the fact that no Raman signal is observed when Ag (Au) nanoparticles are adsorbed on a (4-aminophenyl)silane monolayer assembled on a silicon wafer, the Raman spectrum observed for Ag(Au)@4-ABT/Au(flat) must be a surface-enhanced Raman scattering (SERS) spectrum, derived from the electromagnetic coupling of the localized surface plasmon of Ag (Au) nanoparticles with the surface plasmon polariton of the underneath Au metal. The electromagnetic coupling responsible for SERS appeared to be governed more by the bulk Au substrate than the sparsely distributed Ag or Au nanoparticles. The chemical enhancement appeared on the other hand to be derived more from the formation of Au−S bonds than any charge-transfer interaction between the protonated amine group and the Au or Ag nanoparticles. The enhancement factors derived from the attachment of a single Ag or Au nanoparticle onto 4-ABT on Au were estimated to be as large as 8.3×10^5 and 5.0×10^5, respectively, (for the ring 3 band (b_2) near 1390 cm^{-1}) in which a factor of $\sim 10^2$ was presumed to be due to the chemical effect, with the remaining contributed by the electromagnetic effect.

1. Introduction

Surface enhanced Raman scattering (SERS) is a phenomenon in which the scattering cross sections of molecules adsorbed on certain metal surfaces are dramatically enhanced.[1] In recent years, it has been reported that even single-molecule detection is possible by SERS,[2−4] suggesting that the enhancement factor (EF) can reach as much as 10^{14}−10^{15}; the effective Raman cross sections are then comparable to the usual fluorescence cross sections. SERS had thus been expected to be a useful technique in many areas of science and technology, including chemical analysis, corrosion, lubrication, catalysis, sensor, and molecular electronics, etc.[5−9] However, SERS has not developed to be as powerful a surface technique as many people had initially hoped because of three specific obstacles.[9] One is that only noble metals such as Ag and Au can provide large enhancement effects. Another is that, even for those noble metals, surface roughness on a 50−200 nm scale is crucial for exhibiting a large EF. The other obstacle is that the origin of SERS has not yet been clearly clarified, although electromagnetic (EM) and chemical enhancement mechanisms are definitely responsible for the occurrence of SERS.

In conjunction with single-molecule SERS, an electromagnetic "hot spot" has been predicted to exist in large fractal aggregates of Ag particles.[10,11] The junction of two aggregated Ag nanoparticles has also been claimed to be the "hot" site for SERS.[12] As two particles approach each other, their transition dipoles are expected to couple in such a way that the enhanced EM fields around each particle can create a pattern of coherent interference. This implies that as the distance between the nanoparticles decreases, the coupled plasmon resonance shifts to red, the enhanced EM field increases in the junction between the particles, and destructive interference of the fields occurs at other points in space. For a gap of 1 nm between two Ag spheres that were 90 nm in diameter, the EF was estimated by Xu et al. to be $\sim 10^{10}$ in a volume of space that could contain only a few molecules.[3]

Understanding metal-to-metal interaction is necessary when fabricating functional nanoscale architectures composed of metal particles on the surfaces of solid substrates. When the solid substrate is metallic, not only the interaction between particles but also the interaction between particles and metallic substarte is an important factor determining the opticophysical characteristics of the system. Recent studies on gold colloidal particle-based surface-plasmon-resonance (SPR) devices demonstrate that surface plasmon absorption of a gold substrate can be perturbed by the attached gold colloidal particle monolayer.[13−15] An increased SPR sensitivity to protein−protein interactions has been achieved on such gold colloid particle based substrates. On the other hand, Zheng et al.[16] reported that a SERS spectrum could be obtained for 4-aminobenzenethiol (4-ABT) adsorbed onto a smooth macroscopic silver metal surface by assemblying nanosized Ag particles thereon. The enhancement of the spectrum of 4-ABT was ascribed to an EM coupling of the silver particles and the surface of the silver metal, most probably to the interactions of the localized surface plasmon of the silver particles and the surface plasmon polariton of the silver metal surface.

In this work, we have investigated the optical responses of 4-aminobenzenethiol sandwiched between a macroscopically smooth Au substrate and 55 nm sized Ag or Au nanoparticles. The purpose of the work is to confirm first whether SERS activity is derived from the nanoparticle-to-metal substrate

* To whom all correspondence should be addressed. Phone: +82-2-8806651. Fax: +82-2-8891568. E-mail: kwankim@snu.ac.kr.

10.1021/jp052829b CCC: $30.25
Published on Web 10/14/2005

interaction. Second, it is intended to estimate the EF values associated with the attachment of Ag or Au nanoparticles. Since the gap between the metal nanoparticle and the Au substrate underneath is at best 1 nm, the dependences of EF values on the excitation wavelength, as well as on the kind of metal nanoparticles, are expected to provide valuable information on the nature of hot sites for SERS.

2. Experimental Section

Silver nitrate ($AgNO_3$), hydrogen tetrachloroaurate ($HAuCl_4$), and sodium citrate were purchased from Aldrich and used as received. Other chemicals unless specified were reagent grade, and triply distilled water of resistivity greater than 18.0 MΩ· cm was used throughout.

Au and Ag sols were prepared by following the recipes of Lee and Meisel.[17] Initially, 100 mL of $AgNO_3$ solution (1 mM) was brought to the boil. A solution of 1% sodium citrate (2 mL) was added under vigorous stirring, and boiling was continued for 3 h. For the Au sol, 50 mL of $HAuCl_4$ (0.25 mM) solution and 0.4 mL of sodium citrate (1% (w/v)) were used to obtain Au nanoparticles with sizes comparable to those of Ag nanoparticles; according to transmission electron microscopy (TEM) analyses, the average diameter was 55 nm for both nanoparticles.

Macroscopically smooth Au substrates were prepared by resistive evaporation of titanium and gold at 1×10^{-6} Torr on freshly cleaved mica plates. After a deposition of approximately 200 nm of gold, the evaporator was back-filled with nitrogen. The gold substrates were subsequently immersed in 1 mM of 4-ABT in ethanol overnight. Separately, a (4-aminophenyl)-trimethoxysilane (4-APTMS) monolayer was assembled on a silicon wafer following the protocol in the literature.[18] To attach the Ag or Au nanoparticles to the pendent NH_2 groups, these substrates were soaked in Ag or Au sol for a certain period of time. Even after a prolonged soaking, only a limited number of nanoparticles were adsorbed onto 4-ABT on Au without aggregation. The number of Ag and Au nanoparticles attached to 4-ABT/Au and 4-APTMS/Si were counted using an atomic force microscope (Digital Instruments, Model Nanoscope IIIA). By adjusting the soaking time, ~2 Ag or Au nanoparticles were bound to the pendent NH_2 groups per 1 μm^2 of Au and Si substrates.

For a comparative study, SERS-active Au substrates (0.05 mm thick foil) were also prepared via oxidation−reduction cycles (ORCs) in 0.1 M KCl solution by sweeping consecutively at 1 V/s between −0.8 and +1.0 V versus a standard calomel electrode. 4-ABT was assembled onto these substrates by soaking in 1 mM ethanolic solution overnight.

Raman spectra were obtained using a Renishaw Raman system Model 2000 spectrometer equipped with an integral microscope (Olympus BH2-UMA). The 514.5 nm line from a 20 mW Ar^+ laser (Melles-Griot Model 351MA520) or the 568 nm line from a 20 mW Ar^+/Kr^+ laser (Melles-Griot Model 35KAP431) or the 632.8 nm line from a 17 mW He/Ne laser (Spectra Physics Model 127) was used as the excitation source, and Raman scattering was detected over a 180° range with a Peltier cooled (−70 °C) charged-coupled device (CCD) camera (400 × 600 pixels). The holographic grating (1800 grooves/mm) and the slit allowed the spectral resolution to be 1 cm^{-1}. The Raman band of a silicon wafer at 520 cm^{-1} was used to calibrate the spectrometer, and the accuracy of the spectral measurement was estimated to be better than 1 cm^{-1}. TEM images were obtained with a JEM-200CX transmission electron microscope at 200 kV after placing a drop of the as-prepared sol onto Ni/Cu grids.

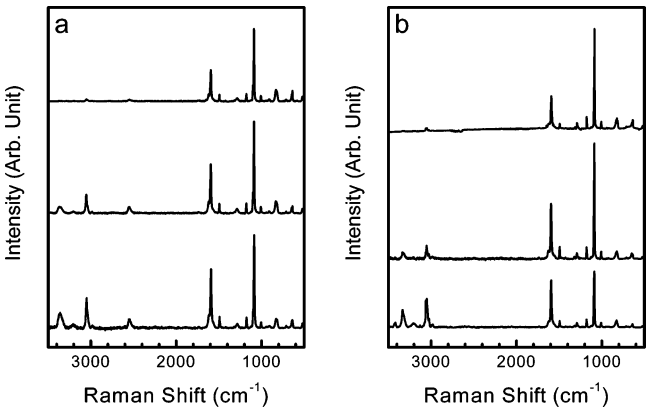

Figure 1. Normal Raman spectra of 4-ABT (a) in neat solid state and (b) in anionic state in alkaline solution, taken using the 632.8 nm line of a He/Ne laser (top), the 568 nm line of a Ar/Kr laser (middle), and the 514.5 nm line of an Ar ion laser (bottom) as excitation sources. All spectral intensities were normalized with respect to those of silicon wafers used for instrument calibration.

3. Results and Discussion

4-Aminobenzenethiol was chosen as a model adsorbate since 4-ABT adsorbs strongly onto Au by forming an Au−S bond.[19] The pendent $-NH_2$ group can subsequently be modified or reacted readily with Ag or Au nanoparticles. For better interpretation of the surface Raman spectra, we first needed to determine the vibrational assignment of 4-ABT in its neat state. Parts a and be of Figure 1 show the normal Raman spectra of 4-ABT in its neat and anionic states, respectively, obtained using 514.5, 568, and 632.8-nm radiation as the excitation sources; the peak intensities, as well as the peak positions, at specific excitation wavelengths were all normalized with respect to the Raman band of a silicon wafer appearing at 520 cm^{-1}. The normalized Raman spectral patterns are barely dependent on the excitation wavelength. Any spectral difference between neat and anionic state is due to the deprotonation of the thiol in the anionic state. Major peaks in Figure 1 are collectively summarized in Table 1 along with their vibrational assignment.[20]

Prior to attempting to record the Raman spectra of 4-ABT assembled on macroscopically smooth Au substrates, we have examined the spectra of 4-ABT assembled on an ORC-treated Au substrate. Figure 2a shows the spectra obtained using 514.5, 568, and 632.8 nm radiation as the excitation sources; once again, all the spectra were normalized with respect to those of silicon wafers. The spectral intensity is seen to be highly dependent on the excitation wavelengths. At 514.5 nm excitation, no peak can be identified. Distinct peaks are observed, however, at 568 nm excitation, and peaks are further intensified at 632.8 nm excitation. As we will discuss later, no Raman peak is identifiable when 4-ABT is assembled on macroscopically smooth Au substrates, even by 632.8 nm excitation, so that the spectra obtained by 568 and 632.8 nm radiation in Figure 2a must be SERS spectra derived from the nanoscaled roughness of the ORC-treated Au substrates. Comparing these with the normal Raman (NR) spectra in Figure 1, the S−H stretching peak is absent in Figure 2a (see the inset), indicating that 4-ABT is adsorbed on Au as a thiolate, as mentioned previously. The absence of the CSH bending band in Figure 2a whose counterpart is clearly seen at ~907 cm^{-1} in Figure 1a also supports the hypothesis of the formation of an Au−S bond, although the Au−S stretching band is barely identifiable in

TABLE 1: Raman Spectral Peak Assignment of 4-Aminobenzenethiol in Free and Surface-Adsorbed States

normal Raman[a]		SERS[a]					
powder	anion state	4-ABT/ Au(ORC)	Ag@4-ABT/ Au(ORC)	Au@4-ABT/ Au(ORC)	Ag@4-ABT/ Au(flat)	Au@4-ABT/ Au(flat)	assignment[b]
	3422vw						
3366vw	3334vw						
3050vw	3052vw						νCH, 2(a_1)
	3031vw						νCH, 13(a_1)
	2990vw						
2551vw							νSH
1737vw	1737vw						
1616w	1627vw						δNH
1593m	1594m		1587w	1587w	1592w		νCC, 8a(a_1)
1570vw	1568vw	1578s	1578s	1578s	1585s	1583s	νCC, 8b(b_2)
			1525vw			1518vw	
1492vw	1495vw	1485w	1487vw	1487vw	1489vw	1487vw	νCC + δCH, 19a(a_1)
		1472vw	1472vw	1472vw	1475vw	1472vw	
1422vw	1423vw	1434m	1436m	1433m	1437m	1434m	νCC + δCH, 19b(b_2)
1367vw	1371vw	1388m	1390m	1388m	1390m	1387m	νCC + δCH, 3(b_2)
		1331w	1329vw	1329w		1329vw	
		1305vw			1311vw		νCC + δCH, 14(b_2)
1286w	1290vw						
			1235vw	1235vw	1233vw		
1176w	1180w	1182m	1186m	1182m	1186m	1180m	δCH, 9a(a_1)
1150vw		1141m	1142s	1140s	1145m	1141m	δCH, 9b(b_2)
1099m	1091m						
1087s	1085s	1076s	1075s	1074s	1079s	1078s	νCS, 7a(a_1)
1008vw	1008vw	1007w	1006w	1006w	1006w	1004w	γCC + γCCC, 18a(a_1)
			959vw	962vw			
		919vw	919vw	919vw	920vw	920vw	πCH, 5b(b_1)
907vw							δSH
829w	828w						
		822vw	818vw	818vw	818vw	818w	
713vw	714vw	712vw	712vw	712vw	714vw	713vw	πCH + πCS + πCC, 4b(b_1)
644w	649w	639vw	641vw	638vw	640vw	639vw	γCCC, 12(a_1)
		545vw	543vw	543vw	544vw	543vw	
519vw	524vw						γCCC, 16b(b_1)

[a] Units in wavenumber (cm^{-1}). [b] Taken from ref 20, denoting the following: ν, stretch; δ and γ, bend; π, wagging; τ, torsion; vs, very strong; s, strong; m, medium; w, weak; and vw, very weak. The ring modes correspond to those of benzene under C_{2v} symmetry.

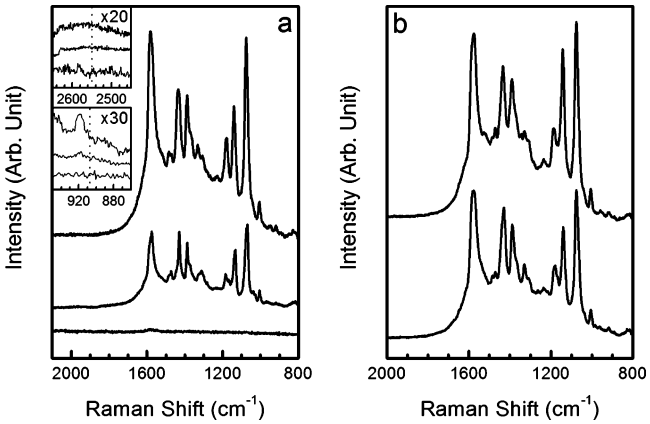

Figure 2. (a) SERS spectra of 4-ABT on ORC-treated Au taken using the 632.8 nm line of a He/Ne laser (top), the 568 nm line of a Ar/Kr laser (middle), and the 514.5-nm line of an Ar ion laser (bottom) as excitation sources. Insets show the spectral regions of SH stretching and CSH bending bands in magnified fashion; their peak positions in normal Raman spectra are marked in dotted lines. (b) SERS spectra of the same system taken after soaking in Ag (upper one) and Au (bottom one) sols using the 632.8 nm line of a He/Ne laser as excitation source. All spectral intensities were normalized with respect to those of silicon wafers used for instrument calibration.

Figure 2a; a weak peak at 919 cm^{-1} in the inset of Figure 2a is due to the ring 5b band and has nothing to do with the CSH bending. Another noteworthy point is that peaks centered at 1578, 1434, 1388, 1182, 1141, and 1076 cm^{-1} are comparatively much stronger than others in Figure 2a. These bands have been identified to belong to either a_1 or b_2 type modes.[20] The enhancement of the a_1 type bands is assumed to reflect a vertical or tilted orientation of 4-ABT on Au. The enhancement of the b_2 type bands is presumably due to the chemical enhancement mechanism associated with the Au-to-4-ABT charge transfer.[20] The peak assignments for the bands in Figure 2a are also made in Table 1.

As mentioned above, no Raman peak is identifiable for 4-ABT assembled on a macroscopically smooth Au substrate. However, distinct peaks can be observed when Ag nanoparticles are attached to the amino group of 4-ABT on Au. As shown in Figure 3a, very distinct spectra are observed, particularly at 632.8 nm excitation. It should be mentioned that only featureless spectra are obtained for 4-aminophenyl silane monolayers assembled on silicon wafers, even after the attachment of Ag nanoparticles onto the terminal amino groups (data not shown).[21,22] This indicates that Ag nanoparticles adsorbed on amino groups are neither hot particles nor hot clusters in exhibiting EM enhancement.[4,23] It also suggests that the chemical enhancement mechanism is insignificant for the electrostatic interaction of Ag nanoparticles with the amino groups. The appearance of Raman peaks in Figure 3a can then be attributed to the electromagnetic coupling of the localized surface plasmon of Ag nanoparticles with the surface plasmon polariton of the smooth Au substrate separated by 4-ABT.

It is noteworthy that the spectral pattern in Figure 3a is almost the same as that in Figure 2a. This implies that the b_2 type bands are notably enhanced upon the anchoring of Ag nanoparticles onto 4-ABT on smooth Au. This does not necessarily mean

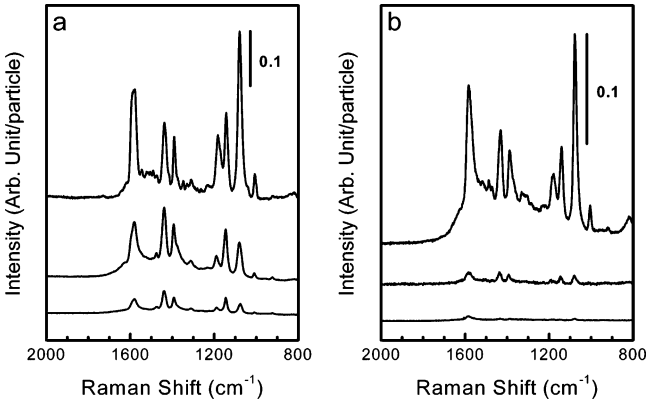

Figure 3. SERS spectra of 4-ABT on flat Au taken after soaking in (a) Ag and (b) Au sols using the 632.8 nm line of a He/Ne laser (top), the 568 nm line of a Ar/Kr laser (middle), and the 514.5 nm line of an Ar ion laser (bottom) as excitation sources.

that the b_2 type band enhancement is caused solely by Ag nanoparticles. To clarify the origin of the excessive enhancement of the b_2 type bands, we have conducted two different experiments. In the first experiment, we have examined what happens if Au nanoparticles are attached onto the amine group of 4-ABT on flat Au. Figure 3b shows the Raman spectra thus obtained at three different excitation wavelengths. The absolute Raman scattering intensity at 568 nm excitation, as well as at 514.5 nm excitation, is fairly weak, but a very distinct and intense spectrum is obtained by the 632.8 nm radiation; the normalized peak intensity in this case is about three-fifths of the case for that of Ag nanoparticle attachment. It is remarkable that the spectral pattern in Figure 3b is nearly the same as that in Figure 3a. That is, the b_2 type bands are also dramatically enhanced by the attachment of Au nanoparticles. Considering the fact that the surface plasmon band of Ag nanoparticles occurs around 420 nm while that of Au nanoparticles is observed at 520 nm, which kind of metal nanoparticle is used seems not to be a crucial factor for the induction of SERS for 4-ABT assembled on macroscopically smooth Au.

To examine whether the excessive enhancement of the b_2 type bands had something to do with the smoothness of the Au substrate, we also obtained the SERS spectra of 4-ABT assembled on an ORC-treated Au substrate by attaching Ag and Au nanoparticles. Figure 2b shows the SERS spectra thus obtained using the 632.8 nm radiation as the excitation source. Surprisingly, the two SERS spectral patterns in Figure 2b are comparable to each other, and they are also comparable to those in Figure 3a,b, as well as to those in Figure 2a. The excessive enhancement of the b_2 type bands would then have to be attributed to an intrinsic character of the basal Au substrate. This possibility is not supported fully by the present experiment, however, since most of the SERS signal in Figure 2b must originate from 4-ABT adsorbed solely on rough Au without attachment of Ag or Au nanoparticles; as discussed below, the surface coverage of Ag or Au nanoparticles is very low.

To evaluate more quantitatively the effectiveness of Ag nanoparticles for the induction of SERS by nanoparticle-to-substrate interaction, we have attempted to use atomic force microscopy (AFM) to count the number of Ag and Au nanoparticles anchored on 4-ABT assembled on smooth Au substrates. As can be seen in the TEM images in the inset of Figure 4, both the Ag and Au nanoparticles are oval shaped with mean diameters of 55 nm; rod-shaped particles are also observed in the Ag sol, occupying ~3% of the total in all. The Ag and Au sols were stable for several weeks, and, more

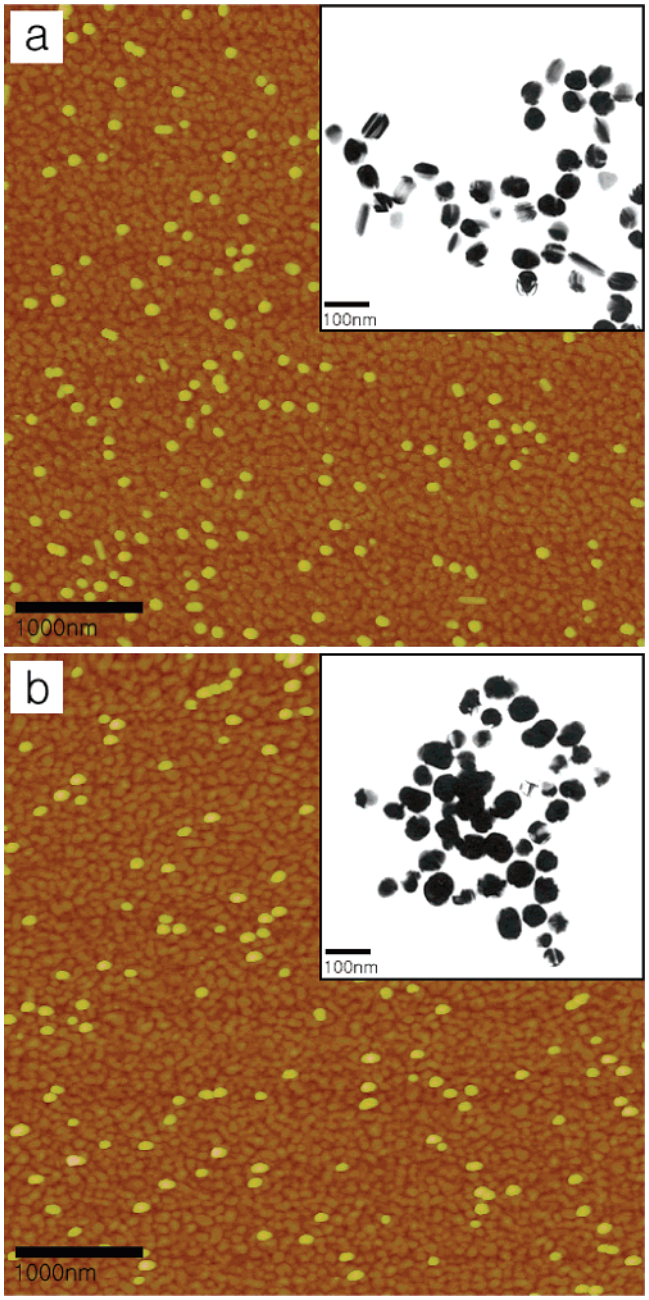

Figure 4. AFM images of 4-ABT SAMs assembled on flat Au after soaking in (a) Ag and (b) Au sols for a prolonged time: Insets are TEM images of (a) Ag and (b) Au nanoparticles in the as-prepared state. When taking spectra in Figure 3, the soaking time was adjusted such that ~2 particles were adsorbed per μm^2 on 4-ABT/Au.

importantly they were hardly subject to aggregation, to the extent that the centrifuged colloids could be re-dispersed in neutral, acidic, and basic solutions, as well as in ethanol and methanol. This may be due to the encapsulation of colloidal particles by negatively charged citrate ions.[24] Considering such electrostatic repulsion, Ag and Au nanoparticles should not bind fully to 4-ABT on Au; the maximum surface coverage attainable is ~10%. On the other hand, since the amine group of 4-ABT on Au is protonated upon soaking in Ag sol, the electrostatic nanoparticle-to-amine interaction must favor the surface adsorption of nanoparticles. Parts a and b of Figure 4 show the AFM images of 4-ABT/Au taken after soaking in Ag and Au sols for a prolonged time (3 h), respectively. Metal nanoparticles are quite evenly distributed over the 4-ABT on Au without aggregation. By adjusting the soaking time, we were able to

regulate the number of Ag(Au) nanoparticles on 4-ABT/Au, and the average surface coverage of Ag(Au) nanoparticles was in fact ~2.0 particles/(1 μm^2) for the samples used to take the Raman spectra, shown in Figure 3a,b.

We have estimated the surface enhancement factor by comparing the peak intensities in Figures 1a and 3a. In conjunction with this, we determined that the sampling volume to obtain the NR spectrum of neat 4-ABT in Figure 1a would be the product of the laser spot (~1 μm in diameter) and the penetration depth (~2 μm) of the focused beam. Since the density of 4-ABT is 1.18 $g \cdot cm^{-3}$,[25] the number of 4-ABT molecules illuminated by the laser light is calculated to be 8.9×10^9 (i.e., 1.5×10^{-14} mol). On the other hand, considering the fact that each 4-ABT molecule occupies an area of ~0.20 nm^2 at the full coverage limit on Au,[26] the number of 4-ABT molecules illuminated by the laser light will be 3.9×10^6 (i.e., 6.5×10^{-18} mol) when taking the Raman spectrum of 4-ABT assembled on flat Au substrates. In this estimation, we ignored the surface roughness of the vacuum-evaporated Au on mica. Since the average surface coverage of Ag nanoparticles was ~2.0/μm^2, the number of Ag nanoparticles illuminated by the laser light would be ~1.6. The number of 4-ABT molecules hidden below those Ag nanoparticles may then be 1.9×10^4 (i.e., 3.0×10^{-20} mol). The intensity ratio of the ring 7a bands (a_1) at ~1080 cm^{-1} in Figures 1a and 3a, taken using 632.8 nm radiation as the excitation source and normalized with respect to the absolute intensity of a silicon wafer, was measured to be 32.2:1. Recalling the fact that the number of 4-ABT molecules illuminated by the laser light in Figure 3a was 3.9×10^6, while that in Figure 1a was 8.9×10^9, the intensity enhancement by the attachment of 1.6 Ag nanoparticles should be ~70, i.e., $(8.9 \times 10^9)/(3.9 \times 10^6 \times 32.2)$. Since the actual number of 4-ABT molecules hidden below the 1.6 Ag nanoparticles is, however, 1.9×10^4, the EF derived solely by 1.6 Ag nanoparticles is estimated to be 1.4×10^4, i.e., $[70/(1.9 \times 10^4/3.9 \times 10^6)]$. The EF achieved by the attachment of a single Ag nanoparticle is then 9.2×10^3, i.e., $(1.4 \times 10^4/1.6)$.

A similar calculation for ring 7a bands leads to a conclusion that the EF achieved by the attachment of a single Au nanoparticle is 5.5×10^3. It has to be mentioned that much larger EF values are obtained for the ring 3 band (b_2) near 1390 cm^{-1}. That is, the EF per attachment of a single Ag nanoparticle is estimated to be 8.3×10^5, while the EF per attachment of an Au nanoparticle is 5.0×10^5. Although these EF values may not be excessively large, it clearly suggests that the crevices or the gaps between two or three nanoparticles in contact with one another are hot sites for the induction of SERS via an EM enhancement mechanism.[4,23]

The notable enhancement of the b_2 type bands among others in the present system could be taken to imply that a considerable portion of the EF was derived from the chemical enhancement associated with the formation of composite bonds in Ag@4-ABT/Au. Considering the fact that the interaction of Ag (Au) nanoparticles with 4-ABT on Au is electrostatic, the chemical enhancement, if it is involved, may occur due to the formation of Au−S bonds rather than the Ag(Au)-to-NH_2 interaction. The observation that Raman spectra could not be obtained for (4-aminophenyl)silane monolayers on Si, even after Ag nanoparticle attachment, supports such a presumption. In the above calculations, the EF value for an a_1 type band was determined to be $(5.5-9.2) \times 10^3$, while that for a b_2 type band was $(5.0-8.3) \times 10^5$. According to the electromagnetic model predicted by Moskovits,[27,28] the a_1 mode should be enhanced more than the b_2 mode, regardless of the orientation of 4-ABT with respect to the metal substrate. However, referring to the Creighton's electromagnetic rule,[29] the EF value of the a_1 type modes can be greater or smaller than that of the b_2 type mode. This is because the a_1 modes are composed of a linear combination of three diagonal elements of Raman tensor. Assuming then that a_1 and b_2 type bands were equally contributed by electromagnetic enhancement, the observed difference in EF values, $\sim 10^2$, would have to be attributed to differences in the extent of CHEM enhancement. That is, the additional EF by a factor of $\sim 10^2$ for the b_2 type mode would be attributed to the chemical effect; if the ring 3a band (a_1 type) was enhanced more by an electromagnetic enhancement mechanism than the ring 7a band (b_2 type), the EF value due to the chemical effect for the ring 7a band should be even greater than 10^2. Recalling the fact that a surface Raman spectrum could hardly be obtained without attaching Ag or Au nanoparticles onto 4-ABT on Au, the chemical enhancement by a factor of $\sim 10^2$ would not be large enough to induce SERS.

4. Summary and Conclusion

Raman scattering measurements were conducted for a 4-ABT monolayer assembled on a macroscopically smooth Au substrate. Although no peak was detected at the beginning, Raman peaks were clearly observed by attaching Ag or Au nanoparticles onto the 4-ABT monolayers. These peaks must have been derived from the electromagnetic coupling of the localized surface plasmon of Ag nanoparticles with the surface plasmon polariton of the Au metal underneath.[13−15] The Raman peaks observed caused by 632.8 nm excitation were ~20 times more intense than those caused by 514.5 nm excitation, suggesting that the electromagnetic coupling responsible for SERS should be governed more by the bulk Au substrate than the sparsely distributed Ag or Au nanoparticles. The spectral pattern itself was also barely different from the usual one observable using rough Au substrates with noticeable enhancement of the b_2 type bands, suggesting that the chemical enhancement was mainly due to the formation of a Au−S bond rather than a charge-transfer interaction between the protonated amine groups and the Au or Ag nanoparticles. The EFs derived from the attachment of a single Ag and Au nanoparticle onto 4-ABT on Au were estimated to be 8.3×10^5 and 5.0×10^5, respectively, for a b_2 type band while the EF values for an a_1 type band were determined to be 9.2×10^3 and 5.5×10^3. The additional EF by a factor of $\sim 10^2$ for the b_2 type mode is attributed to the chemical effect. Finally, the fact that the size of a Ag(Au) nanoparticle (55 nm) was smaller than that of the Ag(Au)-coated AFM tips usually employed in tip-induced SERS; however, the SERS signal was observed only on an Au substrate not on a dielectric silicon wafer, which would indicate that tip-induced SERS should also work well on metallic substrates.

Acknowledgment. This work was supported in part by the Korea Research Foundation (KRF, Grant 2003-015-C00285) and by the Ministry of Commerce, Industry and Energy of the Republic of Korea (Nano Project, M10213240001-02B1524-00210).

References and Notes

(1) Chang, R. K.; Furtak, T. E. *Surface Enhanced Raman Scattering*; Plenum Press: New York, 1982.

(2) Nie, S.; Emory, S. R. *Science* **1997**, *275*, 1102.

(3) Xu, H.; Bjerneld, E. J.; Käll, M.; Börjesson, L. *Phys. Rev. Lett.* **1999**, *83*, 4357.

(4) Futamata, M.; Maruyama, Y.; Ishikawa, M. *Vib. Spectrosc.* **2002**, *30*, 17.

(5) Ni, J.; Lipert, R. J.; Dawson, G. B.; Porter, M. D. *Anal. Chem.* **1999**, *71*, 4903.
(6) Kim, N. H.; Lee, S. J.; Kim, K. *Chem. Commun.* **2003**, 724.
(7) Cao, P.; Gu, R.; Tian, Z. Q. *Langmuir* **2002**, *18*, 7609.
(8) Chu, W.; LeBlanc, R. J.; Williams, C. T.; Kubota, J.; Zaera, F. *J. Phys. Chem. B* **2003**, *107*, 14365.
(9) Tian, Z. Q.; Ren, B.; Wu, D. Y. *J. Phys. Chem. B* **2002**, *106*, 9463.
(10) Markel, V. A.; Shalaev, V. M.; Zhang, P.; Huynh W.; Tay L.; Haslett, T. L.; Moskovits, M. *Phys. Rev. B* **1999**, *59*, 10903.
(11) Bozhelvolnyi, S. I.; Markel, V. A.; Coello, V.; Kim, W.; Shalaev, V. M. *Phys. Rev. B* **1998**, *58*, 11441.
(12) Michaels, A. M.; Jiang, J.; Brus, L. *J. Phys. Chem. B* **2000**, *104*, 11965.
(13) Lyon, L. A.; Musick, M. D.; Natan, M. J. *Anal. Chem.* **1998**, *70*, 5177.
(14) Lyon, L. A.; Pena, D. J.; Natan, M. J. *J. Phys. Chem. B* **1999**, *103*, 5826.
(15) Hutter, E.; Cha, S.; Liu, J.-F.; Park, J.; Yi, J.; Fendler, J. H.; Roy, D. *J. Phys. Chem. B* **2001**, *105*, 8.
(16) Zheng, J.; Zhou, Y.; Li, X.; Ji, Y.; Lu, T.; Gu, R. *Langmuir* **2003**, *19*, 632.
(17) Lee, P. C.; Meisel, D. *J. Phys. Chem.* **1982**, *86*, 3391.
(18) Zhang, F.; Srinivasan, M. P. *Langmuir* **2004**, *20*, 2309.
(19) Ulman, A. *Chem. Rev.* **1996**, *96*, 1533.
(20) Osawa, M.; Matsuda, N.; Yoshii, K.; Uchida, I. *J. Phys. Chem.* **1994**, *98*, 12702.
(21) Chumanow, G.; Sukolov, K.; Gregory, B. W.; Cotton, T. M. *J. Phys. Chem.* **1995**, *99*, 9466.
(22) Grabar, K. C.; Freeman, R. G.; Hommer, M. B.; Natan, M. J. *Anal. Chem.* **1995**, *67*, 735.
(23) Jiang, J.; Bosnick, K.; Maillard, M.; Brus, L. *J. Phys. Chem. B* **2003**, *107*, 9964.
(24) Baudhinm, P., Van der Smissen, P., Beauvois, S., Courtoy, P. J., Hayat, M. A., Eds.; *Colloidal Gold: Principles, Methods, and Applications*; Academic Press: San Diego, 1989; Vol. 2, pp 2−17.
(25) http://www.chemicalland21.com/lifescience/phar/4-AMINOTHIOPHENOL.htm.
(26) Gole, A.; Sainkar, S. R.; Sastry, M. *Chem. Mater.* **2000**, *12*, 1234.
(27) Moskovits, M. *J. Chem. Phys.* **1982**, *77*, 4408.
(28) Moskovits, M. *Rev. Mod. Phys.* **1985**, *57*, 783.
(29) Creighton, J. A. *Surf. Sci.* **1983**, *124*, 209.